Microstructure evolution and damage development in the rails of a single-track railway line after preventive grinding

Schotsman, B.; Huisman, J.; Santofimia, M. J.; Petrov, R. H.; Sietsma, J.

DOI
10.1016/j.wear.2025.206101

Publication date
2025

Document Version
Final published version

Published in
Wear

Wear 576–577 (2025) 206101

Contents lists available at ScienceDirect

Wear

journal homepage: www.elsevier.com/locate/wear

Microstructure evolution and damage development in the rails of a single-track railway line after preventive grinding

B. Schotsman [a,b,*], J. Huisman [a], M.J. Santofimia [a], R.H. Petrov [a,c], J. Sietsma [a]

[a] Delft University of Technology, Department of Materials Science and Engineering, Mekelweg 2, 2628 CD Delft, The Netherlands
[b] ProRail, Moreelsepark 3, 3511 EP Utrecht, The Netherlands
[c] Ghent University, Department of Electrochemical, Systems and Metal Engineering, Technologiepark 46, Ghent, Belgium

ARTICLE INFO

Keywords:
Rail grinding
Single track
Damage
Rail steel
WEL
Rolling direction reversal
Corrugation

ABSTRACT

In sparsely populated areas single-track railway lines are still common. Despite the low-density traffic and low axle loads, rail damage is observed to initiate in the rails of these lines. Not only large cracks requiring repair are found, but also newly initiated, post-grinding damage is observed. Rail specimens from the track containing representative damages are extracted to identify the reasons for the damage initiation in the R260Mn steel rail. At the rail surface, three years after the preventive grinding maintenance, the characteristic grinding facets and roughness patterns are still present. White etching layers are observed to surround the residual grinding grooves, maintaining the roughness as a result of the high wear resistance of these layers. The strain orientation at the gauge side of the rail is uni-directional due to lateral creep in the wheel–rail contact while in the center of the contact surface the strain patterns evidence shear stress reversal associated with the bi-directional traffic. The damage initiation mechanism after preventive grinding is associated with low-wear conditions and stresses concentrated around long-lasting grinding grooves. The findings show that preventive grinding maintenance specifications for regional single-stock railway lines must be improved. Specific points of interest are stringent requirements on the number of facets and surface roughness, as well as directions for the removal of corrugation.

1. Introduction

In sparsely populated areas single-track railway lines between small towns are still common. Trains run in both directions using the same railway track, and pass each other only at larger train stations along the line (see Fig. 1). The service is provided by regional companies and the timetable is simple with one or two trains per direction each hour. The typical single-stock service is operated with light trains designed to meet the travelers' specific local needs. Under these use-conditions the rail wear is low and, as a result, the rail service life long. Despite the low annual track load, damages are detected in the railway rails which require additional rail maintenance and rail replacements. In the following, the available literature on the characteristics of bi-directional use, the resulting wear rate, and the required preventive grinding maintenance on single-track railway lines are discussed with respect to microstructure deformation, damage initiation and propagation under the specific loading conditions.

In the microstructure of the in-service railway rails three zones can be identified. At the surface, to a depth of 50 μm to 150 μm, the plastic deformation is the most severe [1]. Below this zone, the lamellar structure of the pearlitic rail steels is still recognizable and uni-directionally sheared. The angle between the sheared lamellae and the surface is an indication of the deformation severity [2]. At the center of the running surface of the rail the lamellae can even be parallel to that surface [3]. The depth of the region with measurable increase in hardness can vary from 4 mm to 10 mm beneath the rail surface [1,3], which is deeper than the observable deformation. This depth shifts with increasing contact widths [4,5].

Cracks initiated at the surface initially follow the uni-directionally sheared lamellae structure [6]. Simon et al. [7] observed that, within the contact surface, the deformation orientation is not uniformly distributed, introducing new crack-initiation locations.

Under bi-directional use conditions the tangential shear forces exerted on a rail, defining the direction of deformation, are frequently reversed. Tyfour and Beynon [8] and Zeng et al. [9] have shown, in twin disc experiments on pearlitic steels, that reversal starts a process of microstructural re-orientation. The uni-directionally deformed lamellae align with the new shear stress orientation. This process gradually

* Corresponding author at: Delft University of Technology, Department of Materials Science and Engineering, Mekelweg 2, 2628 CD Delft, The Netherlands.
E-mail address: b.schotsman@tudelft.nl (B. Schotsman).

https://doi.org/10.1016/j.wear.2025.206101
Received 24 October 2024; Received in revised form 15 April 2025; Accepted 25 April 2025
Available online 16 May 2025

Fig. 1. Impression of the, non-electrified, single track railway line, Zutphen - Hengelo.

progresses from the surface downwards as the number of revolutions increases. Tyfour and Beynon [10] further showed that cracks, if present, branch after the reversal and realign to the new shear stress orientation.

Rail surface wear is characteristic for railway operations and contributes to the removal of rail damages. On tangent railway tracks the rail wear is already low but Tyfour and Beynon [8] and Zeng et al. [9] observed that frequent rolling direction reversal reduces wear even further. The wear rate drops after the reversal of the tangential shear stress direction and returns to its former rate when the microstructural re-orientation is completed.

Grinding of rails was introduced to re-profile the rail head and correct corrugation wear, already in the 1980s [11]. Nowadays repetitive preventive grinding is a standard maintenance activity and a measure to prevent rolling contact fatigue damage to propagate [12,13]. Rail grinding is regulated by the EN13231-2-standard [14].

The initially continuous rail head contour is approximated by facets after grinding and these facets are defined by grinding grooves perpendicular to the running direction. Both are characteristic of the modern grinding systems with vertical axis orientation of the grinding motors.

The specific energy in grinding is high, compared to other machining operations [15]. Approximately 50% of the input energy is converted to heat during rubbing of the abrasive particles on the surface [16,17]. Surface temperatures will rise above the A_{C3}-temperature, the temperature above which full austenitisation of the microstructure takes place. White etching layer (WEL) is formed during cooling with the rail acting as a heat sink. With the increase in material removal during grinding, and thus the contact pressure of the grinding wheel, the WEL thickness increases [18,19]. The typical hardness of WEL is 2 to 3 times higher than the bulk hardness of the rail steel [20].

Despite the benefits of preventive grinding, the ground surface condition itself may contain defect initiation sites. First, the ground facets are geometric deviations on the rail head. Mesaritis et al. [21], using a full scale test rig, observed flaking defects to initiate at the facet transition zone. Fau et al. [22] observed discrete flaking to initiate from deep grinding grooves at the facet transition zones. Second, the WEL formation results in hard and brittle patches at the rail surface. Cracks in the WEL layer, damage between WEL and the bulk material [23,24], and small WEL stripes that result from singular abrasive particle contact [25] are reported to act as defect initiation sites.

Grinding is not the only cause of WEL formation. It also arises from regular train operations and can take place at the running surface of the rail [26,27]. Sometimes WEL is present together with a brown etching layer (BEL). BEL is observed between the surface WEL and the bulk material or can be directly present at the surface [28]. There is not yet a common view on the mechanism of origin, and different mechanisms are proposed in the literature, like by Li et al. [29], Messaadi and Steenbergen [30], and Al-Juboori et al. [31]. Mattos Ferreira [32] concluded, after performing laser heat treatment experiments, that BEL originates from WEL. The WEL has been tempered during consecutive reheating cycles with lower heat penetration and the different stages of microstructure development in BEL, and hardness along the depth, are strong indicators for this. The BEL hardness is lower than that of WEL but still 1.5–2 times as high as the bulk hardness [29].

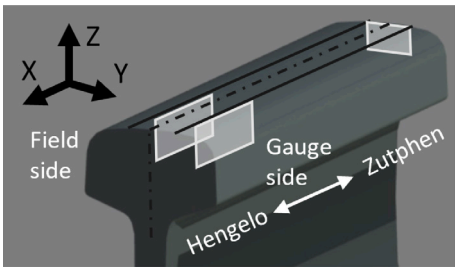

Fig. 2. Scheme of the local coordinate system, and location and orientation of the metallographic cross-sections.

To summarize, the current research interest is on the resulting surface condition after high-powered rail grinding and the effect of the increased grinding frequency on the rail service life. The ground surface may contain, as a result, potential defect initiation sites [21,22,25,33] and well-founded limit values for surface deviations are currently lacking.

This work presents reasons for damage initiation in rails of single-track railway lines subjected to low-frequency, bi-directional traffic after investigating representative rail samples from the single-track railway line Zutphen-Hengelo, in The Netherlands. The surface condition and microstructure of the R260Mn standard-grade rail steel used in that railway line, are analyzed, and the contribution of preventive grinding to the occurrence of surface-initiated damage is considered. This study will add new insight to the discussion on preventive rail grinding design and the critical aspects of the resulting surface, especially for regional single-stock and bi-directional loading conditions.

2. Materials and methods

2.1. Materials

The railway line is a 40 km single-track line, consisting of long tangent track sections and designed to be further developed into a main line, which never happened. The rails are annually inspected to detect rolling contact fatigue damage, to plan corrective maintenance and the necessary renewals. Several locations with rail damage were selected from the inspection reports, and, after day-light inspections, two sections containing representative surface-breaking defects of various sizes, were extracted for this study.

The standard grade R260Mn steel rail used in the line was produced in the Hayange rolling mill in 1992. Table 1 shows the chemical composition ranges and mechanical properties from the EN13674-1-standard [34]. The actual carbon content is 0.62 wt% which is measured using a LECO chemical analyzer. The bulk hardness is 278 ± 8 HV1.

Table 2 shows the traffic data measured using a weighing-in-motion unit on the railway line with 3% measurement accuracy on the single-axle-level. The annual cumulative tonnage is ~1.75 Mt and the line is yearly used by 23540 trains with 157126 axles in total.

The single-stock passenger trains are Alstom LINT 41/H trains which run at $130\,\mathrm{km\,h^{-1}}$ and are equally distributed over both running

Table 1
Chemical composition ranges (wt.%) and mechanical properties of R260Mn rail steel, as stated in the EN13674-1-standard [34].

Chemical composition						Mechanical properties		
C	Si	Mn	P	S	Cr	σ_{UTS} (MPa)	ϵ (%)	Hardness (HBw)
0.53–0.77	0.13–0.62	1.25–1.75	≤0.025	≤0.030	≤0.15	880	10	275–320

Table 2
Total trains and the line load divided into running direction and freight and passenger trains. Measurement period: 10 Sept 2019 – 9 Sept 2020.

Direction		Trains (#)	Axles (#)	Cum. load (kTons)	Axle load Tons($\bar{x} \pm \sigma$)
Hengelo	Passenger	11 608	73 310	797	10.9 ± 0.6
	Freight	162	5174	40	8 ± 5
Zutphen	Passenger	11 604	73 332	796	10.9 ± 0.6
	Freight	166	5310	114	21 ± 2
Total	All	23 540	157 126	1747	

directions. The average axle load of these light vehicles is 10.9 ± 0.6 tons.

The line is also used by a limited number of freight trains. In the direction of Zutphen the locomotives, with a typical axle load of 22 t, pull freight wagons and return empty, as can be concluded from the axle load data presented in Table 2. The freight trains account for only 0.7% of the total number of trains, but due to their length and high axle loads they contribute with 6.5% and 2.3% to the total annual line load, in the respective directions of travel.

When the annual tonnage is extrapolated over the rail life, until the rail replacement in 2020, and assuming that the line load was approximately the same, the total load is ~50 Mt. The replacement took place three years after the last cyclic preventive grinding in 2017 and the analysis was performed in 2022.

2.2. Methods

The analysis of the rails started with the visual observation of the running surface before sectioning. Fig. 2 shows the local coordinate system together with the positions of the micrographs. $Y = Z = 0$ is positioned at the top of the rail profile.

To prepare the specimens, the rails were first cut into slices using a water-cooled BekaMak BMSY 320C band saw. Then the specimens were cut with a Struers Discotom-6 equipped with a ceramic blade. All specimens were mounted with Struers Polyfast and heated and pressed according to the specification of the producer. The surfaces were then prepared using SiC-paper with #80–#4000 grit size and polished with 3 μm and 1 μm diamond polishing fluid. Etching was done with nitric acid, diluted with ethanol (Nital) to 2 vol%, for 10 s.

The observations are made using a Keyence VHX5000 digital microscope and a Jeol JSM 6500F scanning electron microscope, with an acceleration voltage of 15 kV and 9.5 mm working distance, in secondary electron imaging detection mode.

Four sets of hardness measurements were performed using a Struers Durascan 70 hardness tester:

- The first set is made to determine the hardness of the undeformed microstructure using a 10 N load for 10 s.
- Then, the hardness of the running surface is evaluated at the midpoint of the facets and at the facet transition zones. The differences in hardness are used as an estimate of the strain hardening of the rail under cyclic loading. A line of indents is made at seven positions, starting at the surface to $Z = -7$ mm, with an indent spacing of 0.25 mm. In this second set also 10 N load for 10 s is used.
- The aim of the third set is to characterize the observed WEL and BEL layers present at the running surface, using a 0.5 N indenter load.
- The fourth set aims to identify the hardness distribution of the running surface as a result of strain hardening and WEL formation for which a grid of indents with a mutual distance of 5 mm is made. A 30 N load is used for the hardness measurements which limits the observation variations due to local microstructural differences and thin surface layers.

3. Results

3.1. Surface analysis

Fig. 3 shows the ballasted railway track with wooden sleepers on which the rail is mounted with spring clips. The wheel–rail contact surface is light gray and contrasts with the corroded rail. The contact surface has a width of 22 ± 1 mm. At the gauge side of the rail a small secondary contact is observed. The rail is lightly touched by the wheel flange, only removing the surface corrosion.

As a result of the preventive grinding maintenance in 2017, four facets are still present, which are numbered 1 to 4 in this study. The facets are distinguished by the partly worn grinding grooves and the smooth transition zones separating them. Facets 1 and 2, close to the gauge side of the rail, where the rail head radius is small, have a width of 4 mm and 3 mm, respectively. Facets 3 and 4 have a width of 8 mm

Fig. 3. Railway track construction and characteristic contact surface, just before rail sample extraction in 2020. The numbers indicate the ground facets at the contact surface.

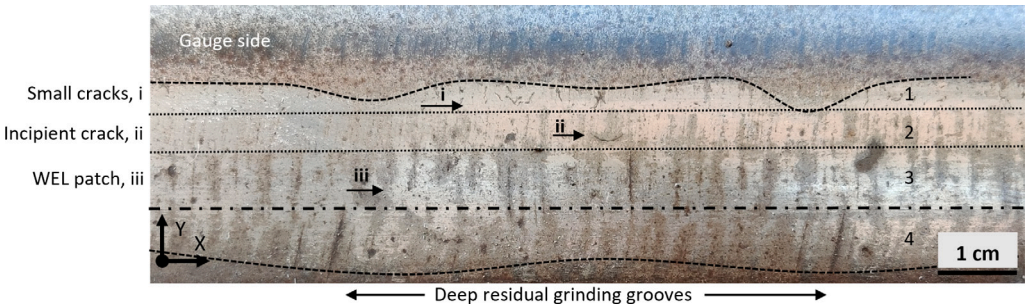

Fig. 4. The rail contact surface as a result of the preventive grinding and wheel–rail contact. The deviations in the contact surface width are depicted with dotted lines. The ground facets are numbered 1 to 4. Small cracks are present at facet 1 (see *i*), an incipient crack at facet 2 (see *ii*), and WEL at facet 3 (see *iii*).

and 7 mm, and are situated on either side of the center line of the rail profile.

Fig. 4 shows a detailed observation of the contact surface in which the facets are also indicated. At the gauge side, next to facet 1, repetitive, localized waves, with an interspacing of 49 ± 2 mm are present. These localized waves are typical for the surface of the rail sections in this study. The surface corrosion visualizing the waves is the result of the absence of wheel contact and is most likely caused by local deviations in the rails' longitudinal profile. The darker spots, outside the contact surface at the gauge side, are formed by repetitive patches of corroded grinding grooves.

At the field side, next to facet 4, a more gradual wave is observed and depicted with a dotted line. A repetitive pattern of notch-like residual grinding grooves decorates the widest points. The notch spacing is 57 ± 1 mm and represents the characteristic length of the preventive grinding process performed at 12 km h^{-1} with a grinding train equipped with 64 grinding motors each operating at 3600 rpm.

On the contact surface, at both sides of the centerline, shiny WEL patches are observed after cleaning and light etching with Nital.

The facets 1 to 4 differ in the depth of the remaining grinding grooves. At facet 2 and especially facet 1, the surface is smooth and the grinding grooves are only recognized by a repetitive pattern in gray or as very shallow wrinkles. At the surface of facets 3 and 4 the pattern is clearly present and some deep, black colored residual grinding grooves are observed.

The damages in the surface of facet 1 are small and show a variety of orientations, whereas in facet 2 a larger incipient crack is observed, indicated with *ii*. Fig. 4 shows that the incipient crack is positioned close to the facet transition zone and between the deep residual grinding grooves at the gauge side of the contact surface.

Fig. 5 shows the surface characteristics at facet 2 and the facet transition zone. The figure presents the surface of the same extracted rail but is taken outside the area shown in Fig. 4, focusing on wider residual grinding grooves in facet 2 and facet 3. Fig. 5A presents the surface after cleaning and light etching and Fig. 5B shows the hardness contour plot which is constructed from a grid of measurements. The grinding grooves and the WEL are readily distinguished as the low-hardness blue and high-hardness yellow/green regions, respectively.

Fig. 5a shows that the residual grinding grooves are surrounded by load-carrying surfaces and that a continuous band of WEL, indicated with *i*, is formed at the facet transition zone between facets 2 and 3. The surfaces of the grinding grooves are darker as a result of the absence of wheel contact and damage initiations, indicated with *ii* and *iii*, are present in the grinding grooves in both facet 1 and facet 2.

Fig. 5b shows that large hardness differences are present in the rail surface, with strong gradients. The highest hardness of ~700 HV indicates the presence of WEL which is supported by the surface observations in Fig. 5a. The crack in facet 2 initiates at the edge of the residual grinding groove.

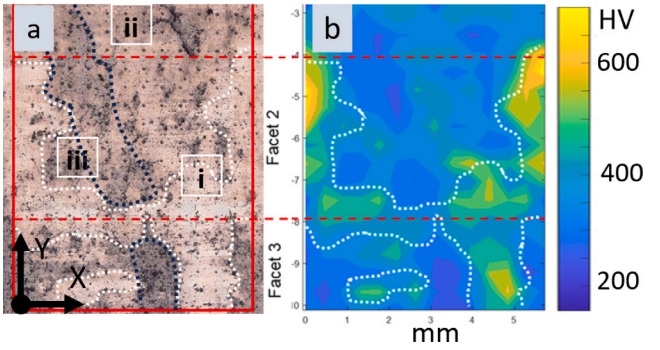

Fig. 5. Detail of the rail surface: (a) Load-carrying surfaces, on which WEL-stripes are present (see i), surround the residual grinding groove, highlighted with dotted lines. In the grinding groove damage initiations are present (see ii and iii). (b) The hardness distribution of that rail surface, showing the locations of lower hardness, the grinding groove (blue) and the locations with higher hardness and WEL (yellow/green). The regions where WEL is observed are outlined by the white dotted lines. (For interpretation of the references to color in this figure legend, the reader is referred to the web version of this article.)

3.2. Large cracks

Investigating the subsurface crack propagation path is one of the objectives of this study. Short cracks propagate along the lamellae orientation of the deformed pearlitic microstructure, preferentially in the pro-eutectoid ferrite [6]. Directionality in longer cracks, for instance the squat defects, is visible in the difference between the leading crack planes and the trailing crack planes. The leading crack plane, in the running direction, propagates over longer lengths and greater depths compared to the trailing crack, developing in the opposite direction [35–37].

Fig. 6 shows a characteristic symmetric squat defect. Fig. 6a presents three of its distinguishing features: (1) the semi-elliptical crack tip with a length of 7 mm, (2) the parallel propagation paths towards the gauge side, and (3) the material extrusion at the side of the contact, where the crack deflects and becomes parallel to the running direction. All features are symmetrical in both running directions, with a slightly more pronounced development in positive X-direction.

Because of the defect size it is concluded that the damage initiation took place before the preventive grinding maintenance was performed. Cracks at the surface tend to shift towards the center line of the rail due to grinding. A displacement as much as 3 mm can occur [38]. The actual position of the semi-elliptical crack tip is close to the facet transition zone between facets 2 and 3.

Fig. 6a shows a dark spot that is formed at the rail surface (see *i*). Locally reduced contact allows for the build-up of intermediate surface layers to form the dark spot. It indicates, together with contact surface widening (see *ii*), the presence of a subsurface crack plane [35]. The increased wheel slip causes longitudinal slip marks (see *iii*), spalling, and

WEL formation. The arrow (see *iv*) indicates the probable displacement of the wheel-contact area.

Fig. 6b shows the subsurface crack plane situated under the dark spot in Fig. 6a. Each line represents a crack contour observed at the milled surface. During each of the first 20 milling passes a layer thickness of 0.05 mm is removed, followed by 0.1 mm per pass until the crack was fully removed. Two additional superficial U-shaped cracks were found close to the crack tip, both initiated at a similar Y-position. These cracks are indicated by the arrow in Fig. 6b.

At a distance from the surface, $Z = -2$ mm, shallow crack branches are found. Crack branching and the subsequent development of parallel crack planes is a known propagation sequence [35]. These secondary cracks initiate at a later crack propagation stage. Therefore crack length and the distance to the surface are no indication for the moment of initiation.

The subsurface crack plane develops in $-Y$-direction, towards the field side of the rail, and in both longitudinal directions. The saddle-shaped plane forms a plateau at a depth of $Z = -3.1$ mm and $Y = -2$ mm. Initially, the crack propagates at a high angle and then deflects to a shallow crack plane orientation of 11°. The crack plane bends upwards at the field side.

The crack plane was assessed on a longitudinal section through both crack tips to study the propagation in the longitudinal directions. The crack plane pointing in X-direction is slightly longer, and from $Z = -4.0$ mm a crack plane propagation angle of 24° is observed. The crack plane reaches a depth of $Z = -5.8$ mm at $Y = 5$ mm. In the opposite direction, at the similar Y-position, a crack plane angle of 30° is found between $Z = -4.0$ mm and $Z = -5.1$ mm. A deflection of the crack at the deepest point of the plane, indicating the onset of growth acceleration, has not been observed in this work.

The observations of the crack propagation path show the symmetry in the subsurface crack planes. Only minor differences in the orientation, length, and depth are present in both longitudinal directions. The equal shape and dimensions, and the initial high propagation plane angle, are notable differences from the observations in rails with unidirectional traffic.

3.3. Cross-section analysis

Cross-sections of the four facets are studied to identify local hardness variations, specific deformation characteristics, and local WEL formation.

Pearlitic rail steels are known for their strain-hardening behavior and the exceedance of the yield limit results in an increase of the hardness and strength [39]. Fig. 7 shows the hardness distribution of the contact surface with in Fig. 7a the measured hardness profiles in blue for facets 1 and 2, and in red for facets 3 and 4. Fig. 7b presents the corresponding measurement positions on the cross-section.

The hardness in facets 1 and 2 is 301 ± 7 HV close to the surface and decreases gradually to the measured bulk hardness at a distance of 5 mm. The hardness at facets 3 and 4 only shows an increase at a distance 3 mm to 4 mm while close to the surface no increase in hardness is measured. The hardness variation in the running surface is an indication of uneven contact stress distribution in the running surface. The subsurface increase is most likely caused by the maximum subsurface stress from the wheel–rail contact patch [4].

Figs. 8a–d show the cross-section of facets 1 to 3 to observe the surface, which is virtually free of corrosion, and the microstructure. Fig. 8a presents the facet transition zone between facets 2 and 3. Locally no WEL is present at the surface. The WEL detachment, indicated in the figure, forms a damage initiation site that has been reported in the literature [24,28,40].

Figs. 8b and 8c show the surface of facet 2. The lens-shaped WEL at the surface is embedded in a BEL, evidencing a history of slip events. The crack in Fig. 8b starts at a corrosion pit and propagates through these layers, but the stresses do not exceed the critical level to grow the crack into the bulk material. This is highlighted by the inserted SEM image in which the lines depict the WEL and BEL boundaries.

In facet 2, close to facet 1, the lens-shaped WEL is partly embedded in BEL, which is in Fig. 8c indicated with *i* and *ii*, respectively.

Fig. 8d shows the surface of facet 1. This surface is WEL free and subsurface deformation is present. The deformation orientation is in Y-direction, towards the gauge side of the rail, see *i*, and the maximum depth of deformation is ~50 µm. The orientation suggests the presence

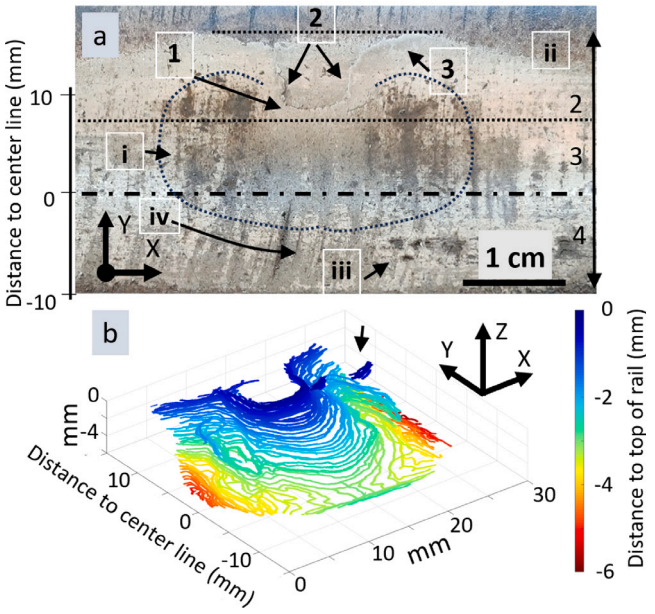

Fig. 6. A symmetric squat defect with semi-elliptical crack tip: (a) Three distinguishing features are indicated: (1) the semi-elliptical crack tip, (2) the parallel propagation paths, and (3) the deflection of the crack path. The dark spot (see *i*) is the result of intermediate-layer build-up and evidences the subsidence of the surface. The contact surface shows contact surface widening (see *ii*), longitudinal slipmarks (see *iii*), and spalling of material. The arrow indicates the probable wheel-contact displacement (see *iv*). (b) 3D-representation of the subsurface crack plane composed of all contour lines after surface milling. The arrows indicate crack initiations present at a similar transverse position.

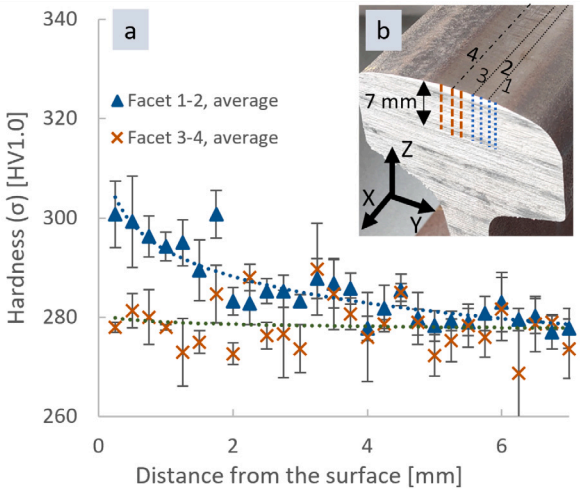

Fig. 7. The hardness distribution below the running band: (a) graph presenting the hardness measured on the cross-section of facets 1 and 2 in blue and facets 3 and 4 in orange. The hardness is measured from a distance of 0.25 mm to the surface, until 7 mm distance. (b) The location of the hardness indents on the cross-section. The colors correspond with the colors in the graph. (For interpretation of the references to color in this figure legend, the reader is referred to the web version of this article.)

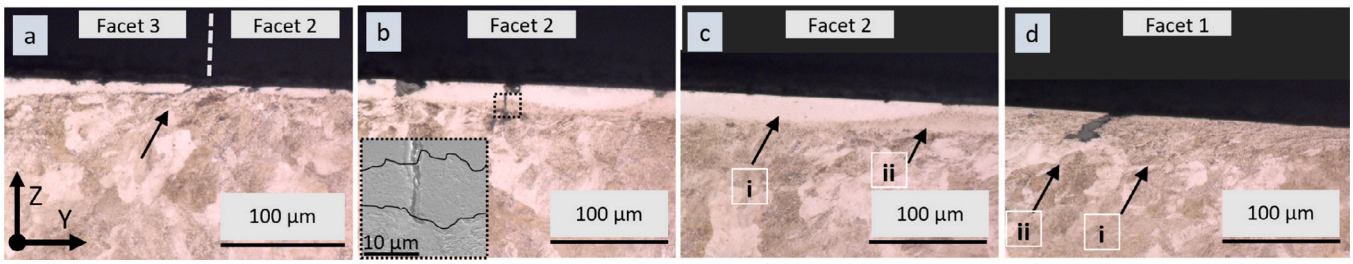

Fig. 8. Cross-section of facets 1 to 3 observed in X-direction: (a) At the facet transition zone between facets 2 and 3 is locally no WEL observed. WEL-detachment is indicated with the arrow. (b) WEL is present at the surface of Facet 2. The observed crack does not propagate into the bulk. (c) WEL is present (see *i*) and partly embedded in BEL (see *ii*). (d) Unidirectional deformation is present beneath the surface of facet 1 (see *i*), and a superficial crack is present (see *ii*).

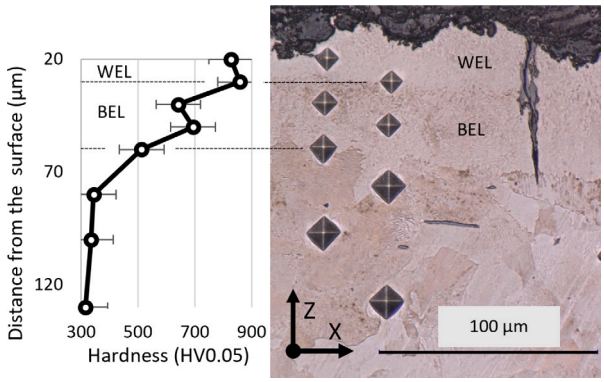

Fig. 9. Longitudinal section of Facet 2, closest to the facet transition with facet 3. A 80 µm corroded WEL and BEL is present at the surface. The graph presents the measurement results at the corresponding measurement positions.

of a shear stress component in the wheel–rail contact that points in that direction. The superficial crack, indicated with *ii*, is one of the many cracks observed in facet 1.

3.4. Longitudinal section analysis

Fig. 9 shows the micrograph of the surface condition in facet 2, closest to the transition to facet 3. Although the WEL surface is corroded, the presence of thick WEL and BEL indicates a history of wheel slip events. The total thickness of WEL and BEL is ~80 µm, allowing hardness measurements to be carried out. The hardness of the WEL is 828 HV, which increases to 859 HV at the WEL–BEL interface. The hardness of the BEL is significantly lower, between 650 HV and 700 HV. WEL and BEL layers are prone to crack initiation [23,31,40]. In this micrograph a crack is present, which is one of a group of closely clustered cracks. None of these cracks propagates into the bulk material.

Fig. 10 shows micrographs from the same specimen as shown in Fig. 9. Fig. 10a presents the surface which is defined by a rough zone next to a WEL. The WEL has a smooth surface and is ~3 µm thick. The pearlite lamellae at the edge of the layer, indicated with *iii*, are wrinkled. The rough zone is filled with debris and detached layers, see *ii*, which is an indication of the absence of wheel contact. Two cracks are observed, although some over-etching limits the observation clarity. The first crack initiates at the bottom of the irregularity, and the second at the edge of the WEL patch, which is indicated with *i*. It is known that the dominant direction of the tangential shear forces defines the deformation orientation [24,27,31] and also that, in this study, the shear stress direction reverses after almost every train passage. Fig. 10b shows the microstructure close to the surface. A 10 µm refined surface layer is present which is the result of intense plastic deformation [1,7]. Wear tongues are pointing in the X-direction, see *i*. The full black line highlights the long C-shaped deformation with a sharp S-shaped pattern, closer to the surface. This pattern is concentrated in a band which is marked by a dotted line. Wrinkled lamellae are sometimes observed in pearlite as a result of compression or thermal contraction. The wrinkled lamellae, indicated with *ii*, show evidence of multiple deflection occurrences and it is concluded from the sharp bending and amplitude variations that these are the result of external shear stress reversal. This specific pattern was also observed by Tyfour and Beynon [10] in rolling direction reversal experiments.

4. Discussion

The contact surface condition that is characteristic of this railway line is the result of the rail maintenance and the single-stock and bi-directional use. In this section the observed inhomogeneous wear, surface hardening, and damage initiation mechanisms are discussed with respect to the low axle load, low traffic density and observed damage.

4.1. Inhomogeneous wear and loading

Preventive maintenance grinding was performed in 2017 and ~5 Mt of train traffic has rolled over the ground surface until the rail sections are extracted in 2020. The grinding maintenance has introduced facets on the surface which are recognizable by the presence of grinding grooves having similar orientations. Fig. 4 shows that the surfaces of the transition zones between the facets are relatively smooth. At the surface of facets 1 and especially 2, some remains of the grinding-related roughness are present, whereas at facets 3 and 4, transverse grooves are still shown and surrounded by a rougher surface. These differences in surface condition are the result of local differences in rail wear.

With the simple wear law of Archard, $Q = KWL/H$ [41], the wear volume Q is predicted from the loading conditions, normal force W and sliding distance L, and H the surface hardness. K is a constant. The wear law therefore predicts the highest wear rate for locations with the highest value of WL in the wheel–rail-contact.

The normal load and the micro-slip in the wheel–rail contact are not homogeneously distributed as a result of the conical wheel tread and the rail-head curvature, resulting in hardness differences of that surface. High hardness is expected when WL is high, no increase in hardness is expected when WL is low.

Fig. 7 shows the hardness distribution along the contact surface. The bulk hardness of the R260Mn rail steel is 278 ± 8 HV 1 and it is observed that the same hardness is present at facets 3 and 4. But in facets 1 and 2, where also numerous small surface cracks are observed, the hardness is higher. From the observed differences in hardness, and the observed microstructure deformation in facets 1 and 2, it is concluded that WL is higher in facets 1 and 2 compared to 3 and 4.

Tyfour and Beynon [8] observed that the unidirectionally strained pearlite starts to realign with the new shear stress direction after reversal of the rolling direction. It is therefore expected that the bi-directional traffic conditions result in the reorientation of the microstructure. More importantly, Tyfour and Beynon [8] also observed a temporary but significant reduction in wear rate after rolling direction

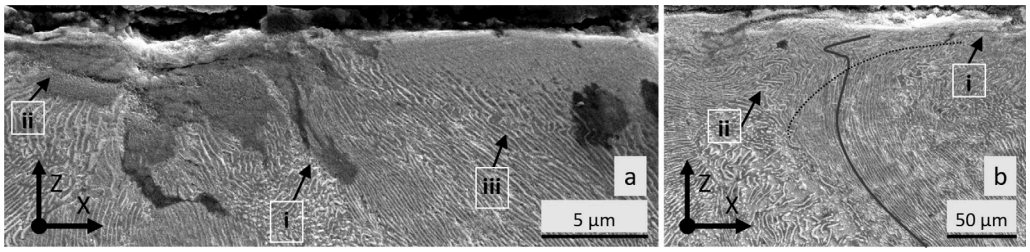

Fig. 10. Longitudinal section of Facet 2, closest to the facet transition with facet 3. The observations are made using high-magnification SEM: (a) Damage initiates (see *i*) between the oxide-filled irregularity (see *ii*) and the WEL patch at the contact surface. Wrinkled pearlite lamellae are present at the edge of the WEL (see *iii*). (b) A wear tongue and s-shaped deformation patterns, associated with the bi-directional use of the railway line, are present (see *i*). Wrinkled pearlite lamellae evidences multiple deflection occurrences (see *ii*).

reversal, which only raised to the former level when the realigning was completed.

The uniform straining of the pearlite lamellae in the microstructure at facets 1 and 2 is directed towards the gauge side of the rail. This deformation orientation is the result of the running-direction independent lateral slip, which is always directed towards the track center. The slip forces in the wheel–rail contact play an important role in the guidance and stable running of trains [4]. Johnson [4] has made a distinction in slip directions. Longitudinal micro-slip, in X-direction, lateral micro-slip, in Y-direction, and spin. Longitudinal micro-slip is the result of traction and braking. The lateral micro-slip results from small yaw angles between the plane of the wheel and the rail and contributes to the self-centering of the wheelset. Spin is the angular velocity relative to the rail, which occurs when the plane of the contact is not parallel to the wheelset axis of rotation, i.e. the axle. Spin is typically strongest at the gauge corner and the gauge face.

The deformation beneath the surface at the contact extreme at the gauge side can be explained as follows. With the change in running direction, it is evident that the traction direction changes as well, and, as a result, the longitudinal micro-slip direction. The self-centering forces, in Y-direction, balance the train, supported by conical wheels mounted on a rigid axle, between the two rails. The lateral slip direction is therefore independent of the running direction and causes the deformation orientation as observed at facets 1 and 2.

The frequent reversal provides a reliable explanation for lower wear in the contact center while the higher load and the unidirectional share in the slip cause a relatively high wear rate. These different loading conditions on the top of the rail and in facets 1 and 2 explain the observed inhomogeneous wear of the rail surface.

4.2. Waviness and WEL formation

Waviness is observed at both sides of the running surface, indicating a variation in the contact surface width. This variation in width is, in itself, a result of a periodic irregularity in the longitudinal rail profile, a surface topography with ripples [42]. The highest points are indicated as ‘hill’ and the lowest as ‘valley’. The presence of these ripples cause differential wheel–rail contact conditions.

The periodic deep residual grinding grooves in facet 4 indicate that this is the characteristic length of the preventive grinding. Between both grooves in facet 4, in adjacent facet 3, a sharp notch is present, indicating a pattern shift between both facets. This pattern shift in single-pass grinding is caused by the longitudinal placement of the multiple grinding motors in the grinding train. The wavelength at the gauge side of the rail, being 49 ± 2 mm, is shorter. This wavelength might be caused by prior grinding maintenance. However, the absence of repetitive grinding grooves could also point to short-pitch corrugation as the cause.

Short-pitch corrugation is a differential rail wear mechanism resulting in a periodic irregularity of the contact surface. Grassie and Kalousek [43] showed rail corrugation wavelengths from 500 mm to 1500 mm for light-rail railway lines. These wavelengths are caused by P2-resonance which occurs when the unsprung mass of the train excites the track. Li et al. [44] observed that the wavelength is best explained by the pinned–pinned frequency of the rail itself, which is 400 Hz to 1200 Hz. This frequency range corresponds, at the line speed of 130 km h^{-1}, with a wavelength of 30 mm to 90 mm. Short-pitch corrugation is generally observed to have a pitch of 25 mm to 80 mm [44,45].

When a periodicity in the longitudinal profile is present, the resulting contact stress variations will also cause differences in the rail surface. Wild et al. [42] studied the rail surface with severe, 35 mm wavelength, short-pitch-corrugation. They observed WEL to be present at the hill of the ripple, while in the valley strong plastic deformation is observed. The WEL, as observed by Wild et al. [42], is lens-shaped, shows an abrupt transition to the bulk and has a hardness between 767 HV and 915 HV. Steenbergen and Dollevoet [23] and Pan et al. [27] have attributed these characteristics to WEL that is wheel-slip induced.

Crack initiation at the ‘hill’ of the rail corrugation is observed in high-speed railway lines, and is named ‘belgrospi’ after Belz, Grohmann, and Spiegel [46]. It is in this study shown that WEL is present at hill parts of the running surface, which is in agreement with the observations by Wild et al. [42]. Although researchers like Steenbergen and Dollevoet [35], Lian et al. [24], Mojumder et al. [28], and Carroll and Beynon [47], associate the presence of the hard and brittle WEL in itself with defect initiation, the cracks in the WEL and BEL layers in this work are not observed to penetrate into the bulk material. Therefore, it is concluded that a different mechanism takes place.

The incipient crack has initiated in the valley of the corrugation wave at the running surface, as shown in Fig. 4. Wild et al. [42] showed that wheel–rail contact in the valley zones results in lamellae that are strained parallel to the surface. Rolling contact fatigue cracks tend to initiate between these elongated lamellae. Simon et al. [7] studied the strain orientation within the rail steel to explain the incipient squat initiation position. They observed that the deformation underneath the contact surface is not uniform as a result of the shear orientation distribution in the wheel contact. Squats are found to initiate preferentially at positions where bands with opposing deformation orientations meet.

Observations on the metallographic cross-sections have shown that, as a result of the bi-directional traffic conditions, different deformation orientations meet at the initiation position of the incipient crack in facet 2, closest to facet 3. The deformation in the lateral direction, as observed in Fig. 8, is reinforced with every train passage, independent of the running direction. This deformation is also evidenced by the local increase in hardness, as shown in Fig. 7. In the longitudinal direction is only shallow C-shaped deformation is present.

4.3. Damage mechanism

At the rail surface a global and a local damage mechanism are observed. In the previous section the focus was on short-pitch corrugation and the associated WEL and deformation, which are collectively considered the global mechanism facilitating damage initiation.

The specific local surface conditions, at the damage initiation position of the incipient crack, are examined in more detail. This is of interest since the large cracks appear to have initiated at a similar position.

Local damage formation has been explained by different researchers based on different aspects of surface conditions. Steenbergen and Dollevoet [23] and Mojumder et al. [28] observed damage to initiate at, or close to the interface between the WEL patch that is formed at the surface, and the deformed material that is surrounding it. Deng et al. [38] studied a different mechanism. They observed that defects may initiate due to the local contact stress concentration at the edge of a depression when it is present on the running surface.

The surface condition after grinding was studied by various researchers to explain grinding-related damage initiations. Fau et al. [22] and Mesaritis et al. [21] observed that contact stress concentrations in the facet transition zone may result in damage initiation. The differences in shear stress orientation at the surface, as previously mentioned, cause different strain orientations. Simon et al. [7] observed squats to initiate at the interface of bands having opposing deformation orientations.

Specific for the damage initiation position in facet 2, closest to facet 3, is that it may be considered the transition between the surface condition formed under the influence of rolling direction reversal and the surface condition that is the result of lateral slip. Tyfour and Beynon [8] experimentally observed a reduction in the wear rate directly after rolling direction reversal, which may contribute to the formation of the surface condition.

Although the surface at facet 2 is relatively smooth, residuals of the grinding roughness are still locally present. These residual grinding grooves are surrounded by WEL-coated contact surfaces.

The local damage mechanism is related to the surface condition that arises after grinding. Under the specific loading conditions, wear is insufficient to remove the grinding roughness completely. And when there is a build-up of WEL in a region of residual grinding grooves, it is observed that cracks typically initiate at the root of the groove close to the facet transition. The surface crack subsequently follows the edge of the grinding groove.

4.4. Crack propagation

The low-axle load and bi-directional traffic influence the crack propagation in two ways. First, under the bi-directional traffic conditions no dominant running direction is present. Second, a crack plane orientation, due to the presence of only shallow wrinkled lamellae, is not evident.

Zerbst et al. [5] observed that, at shallow depth, the crack propagation plane is mostly defined by the shear stress orientation and is therefore expected to propagate in the running direction first. In most cases the propagation is at a 10° to 20° angle with the surface, and deflects at a limited depth to follow an approximately 35° propagation angle. Also Grassie et al. [48] and Steenbergen and Dollevoet [35] observed, under uni-directional traffic conditions, a shallow angle crack propagation plane close to the surface.

Although both the preventive grinding maintenance and wear have changed the surface and removed the actual damage initiation conditions, the 3D-representation of the crack plane in Fig. 6B shows that the crack propagation angle, directly beneath the surface, is relatively high. No deflection of the crack plane occurs until a crack depth of ∼2 mm is reached. Tyfour and Beynon [10] observed that, after rolling direction reversal, cracks re-initiated and branched to align with the reversed stress orientation. Re-initiation takes time and may not occur due to the frequent reversal of the shear stress. Under these conditions, a relatively steep crack orientation may occur. The subsurface propagation is not guided by the deformed lamella orientation as a consequence of the limited microstructural deformation but by the principal stresses only.

At the railway line the passenger trains are symmetrically distributed in number and weight, only the freight trains running to Zutphen have a significantly higher axle load. The crack plane orientations pointing in both running directions are fairly symmetric, although the increased traction forces may explain the observed difference in propagation plane angle, as, provided uni-directional rolling conditions, a leading crack plane of a squat or stud rail defect, pointing in the running direction, is longer and deeper compared to the steep trailing crack plane, propagating against the running direction [35–37,48].

The observed crack plane in Fig. 6, propagating in Y-direction, towards the field side of the running surface, shows an angle of 11° with respect to the horizontal plane and reaches a depth of 3.1 mm. The cracks that propagate beyond that depth do not longer form a continuous contour, and the crack planes in both longitudinal directions are not connected anymore. The crack plane branches to a more shallow propagation angle of 30° in $+X$-direction, the direction of Hengelo and −24° in $-X$-direction, towards Zutphen. It is known that the increase in traction, and therefore in tangential shear stress, moves the principal shear stress to the surface [4], and in these situations, the subsurface cracks tend to propagate at a shallow angle, although with depth the influence of shear stress and contact stress diminishes. Bending and mode II shear become more important [5].

Tyfour and Beynon [10] observed cracks to branch, in rolling-direction reversal experiments, aligning with the new shear stress orientation. In this study no crack path re-orientation is observed which may be caused by the frequent reversions and the limited number of load cycles to re-initiate a new crack path. The crack plane being steep-angled may nevertheless be explained by the crack path re-orientation mechanism.

5. Conclusions

The main purpose of the present work is to identify the reasons for damage initiation in rails of single-track railway lines. It is concluded that:

- The running surface sees differential wear rates. Facets and grinding grooves of preventive grinding maintenance are still present at the center of the contact surface after ∼5 Mt of train load, but are worn off at the gauge side. S-shaped deformation of the lamellae underneath the contact surface is caused by the reversal of the shear stress. The hardness increase below the center of the contact surface is small, and the thick WEL indicates the presence of strong wheel slip. The pearlite lamellae show unidirectional strain deformation close to the gauge side which is explained by the rolling-direction independent lateral slip in the wheel–rail contact.
- At the contact surface of the rail a global and a local damage mechanism are observed. The global damage mechanism is caused by corrugation. Corrugation was not entirely removed during the last preventive maintenance grinding cycle. As a consequence of the longitudinal waviness in the rail surface, WEL patches emerge at the hill part of the ripple. A novel observation is the damage initiation in the valley part of the rail corrugation.
- The local damage mechanism is related to the surface condition that arises after grinding. Under the specific loading conditions, wear is insufficient to remove the grinding roughness completely. Before the roughness is removed, WEL builds up around the grinding grooves and damage may initiate as a result of stress concentration at the facet transition and WEL interface.
- The symmetric squat defect mapped in Fig. 6 develops a subsurface saddle shape, displaying crack propagation in lateral and both longitudinal directions. The ‘crack saddle’ reaches a depth of 3.1 mm, and bends upwards at the field side. Beyond that depth, independent crack propagation takes place in both running directions. The observed close similarity in crack plane lengths and angles is explained by the bi-directional traffic, causing crack growth under reversing shear stresses of equivalent magnitudes.

- The preventive grinding maintenance specifications for regional railway lines must be improved based on the observations in this study. Stringent requirements on surface roughness and the minimum number of facets will reduce the number of potential crack initiation sites. These specifications should also include directions for the removal of short-pitch corrugation. Moreover, the presence of corrugation requires additional material removal to avoid damage to initiate in the ripple valley.

CRediT authorship contribution statement

B. Schotsman: Writing – original draft, Methodology, Formal analysis, Data curation, Conceptualization. **J. Huisman:** Writing – review & editing, Visualization, Investigation, Conceptualization. **M.J. Santofimia:** Writing – review & editing, Visualization. **R.H. Petrov:** Writing – review & editing. **J. Sietsma:** Writing – review & editing, Supervision.

Declaration of competing interest

The authors declare that they have no known competing financial interests or personal relationships that could have appeared to influence the work reported in this paper.

Acknowledgments

This research was carried out under project number T18014 in the framework of the Partnership Program of the Materials innovation institute M2i (www.m2i.nl). We would like to thank ProRail for its financial support and Volker Rail for their support and for arranging inspections and the rails for this research.

Data availability

The raw/processed data required to reproduce these findings are available on request.

References

[1] F.A. Alwahdi, A. Kapoor, F.J. Franklin, Subsurface microstructural analysis and mechanical properties of pearlitic rail steels in service, Wear 302 (1–2) (2013) 1453–1460, http://dx.doi.org/10.1016/j.wear.2012.12.058.

[2] W.R. Tyfour, J.H. Beynon, A. Kapoor, Deterioration of rolling contact fatigue life of pearlitic rail steel due to dry-wet rolling-sliding line contact, Wear 197 (1996) 255–265, http://dx.doi.org/10.1016/0043-1648(96)06978-5.

[3] B. Dylewski, M. Risbet, S. Bouvier, The tridimensional gradient of microstructure in worn rails – Experimental characterization of plastic deformation accumulated by RCF, Wear 392–393 (2017) 50–59, http://dx.doi.org/10.1016/j.wear.2017.09.001.

[4] K.L. Johnson, Contact Mechanics, Cambridge University Press, 1985, http://dx.doi.org/10.1017/CBO9781139171731.

[5] U. Zerbst, R. Lundén, K.O. Edel, R.A. Smith, Introduction to the damage tolerance behaviour of railway rails - a review, Eng. Fract. Mech. 76 (17) (2009) 2563–2601, http://dx.doi.org/10.1016/j.engfracmech.2009.09.003.

[6] J.E. Garnham, C.L. Davis, Very early stage rolling contact fatigue crack growth in pearlitic rail steels, Wear 271 (1–2) (2011) 100–112, http://dx.doi.org/10.1016/j.wear.2010.10.004.

[7] S. Simon, A. Saulot, C. Dayot, X. Quost, Y. Berthier, Tribological characterization of rail squat defects, Wear 297 (1–2) (2013) 926–942, http://dx.doi.org/10.1016/j.wear.2012.11.011.

[8] W. Tyfour, J. Beynon, The effect of rolling direction reversal on the wear rate and wear mechanism of pearlitic rail steel, Tribol. Int. 27 (6) (1994) 401–412, http://dx.doi.org/10.1016/0301-679X(94)90017-5.

[9] D. Zeng, L. Lu, J. Zhang, X. Jin, M. Zhu, Effect of bi-directional operation on rolling-sliding wear of wheel steel under variable amplitude loading, Proc. Inst. Mech. Eng. Part J: J. Eng. Tribol. 230 (2) (2016) 186–195, http://dx.doi.org/10.1177/1350650115594955.

[10] W. Tyfour, J. Beynon, The effect of rolling direction reversal on fatigue crack morphology and propagation, Tribol. Int. 27 (4) (1994) 273–282, http://dx.doi.org/10.1016/0301-679X(94)90007-8.

[11] R. De Vries, P. Sroba, E. Magel, Preventive grinding moves into the 21 st century on Canadian Pacific railway, in: Proceedings from the AREMA Annual Conference, Chicago, IL, 2001.

[12] E. Magel, M. Roney, J. Kalousek, P. Sroba, The blending of theory and practice in modern rail grinding, Fatigue Fract. Eng. Mater. Struct. 26 (10) (2003) 921–929, http://dx.doi.org/10.1046/j.1460-2695.2003.00669.x.

[13] S. Grassie, Rolling contact fatigue on the British railway system: treatment, Wear 258 (7–8) (2005) 1310–1318, http://dx.doi.org/10.1016/j.wear.2004.03.065.

[14] CEN, EN13231-2 - Railway Application - Track - Acceptance of Works - Part 2: Acceptance of Reprofiling Rails in Plain Line, Switches, Crossings and Expansion Devices, CEN, 2020.

[15] S. Kalpakjian, S. Schmid, K. Vijay Sekar, Manufacturing Engineering and Technology, 7th SI Edition, seventh ed., Pearson, 2014, p. 1224.

[16] A. Darafon, A. Warkentin, R. Bauer, 3D metal removal simulation to determine uncut chip thickness, contact length, and surface finish in grinding, Int. J. Adv. Manuf. Technol. 66 (9–12) (2013) 1715–1724, http://dx.doi.org/10.1007/s00170-012-4452-1.

[17] S. Malkin, C. Guo, Thermal analysis of grinding, CIRP Ann 56 (2) (2007) 760–782, http://dx.doi.org/10.1016/j.cirp.2007.10.005.

[18] B. Lin, K. Zhou, J. Guo, Q. Liu, W. Wang, Influence of grinding parameters on surface temperature and burn behaviors of grinding rail, Tribol. Int. 122 (2018) 151–162, http://dx.doi.org/10.1016/j.triboint.2018.02.017.

[19] E. Uhlmann, P. Lypovka, L. Hochschild, N. Schröer, Influence of rail grinding process parameters on rail surface roughness and surface layer hardness, Wear 366–367 (2016) 287–293, http://dx.doi.org/10.1016/j.wear.2016.03.023.

[20] J. Wu, R.H. Petrov, M. Naeimi, Z. Li, R. Dollevoet, J. Sietsma, Laboratory simulation of martensite formation of white etching layer in rail steel, Int. J. Fatigue 91 (2016) 11–20, http://dx.doi.org/10.1016/j.ijfatigue.2016.05.016.

[21] M. Mesaritis, J.F. Santa, L.F. Molina, M. Palacio, A. Toro, R. Lewis, Post-field grinding evaluation of different rail grades in full-scale wheel/rail laboratory tests, Tribol. Int. 177 (2023) http://dx.doi.org/10.1016/j.triboint.2022.107980.

[22] F. Fau, H. Smith, S. Fretwell-Smith, L. Deng, Effect of grinding quality, lubrication quality and rail hardness on flaking defect initiation on high rails, in: Proceedings of the 10th International Conference on Contact Mechanics and Wear of Rail/Wheel Systems, CM2015, 2015.

[23] M. Steenbergen, R. Dollevoet, On the mechanism of squat formation on train rails - Part I: Origination, Int. J. Fatigue 47 (2013) 361–372, http://dx.doi.org/10.1016/j.ijfatigue.2012.04.023.

[24] Q. Lian, G. Deng, A. Al-Juboori, H. Li, Z. Liu, X. Wang, H. Zhu, Crack propagation behavior in white etching layer on rail steel surface, Eng. Fail. Anal. 104 (2019) 816–829, http://dx.doi.org/10.1016/j.engfailanal.2019.06.067.

[25] C. Rasmussen, S. Fæster, S. Dhar, J. Quaade, M. Bini, H. Danielsen, Surface crack formation on rails at grinding induced martensite white etching layers, Wear 384–385 (2017) 8–14, http://dx.doi.org/10.1016/j.wear.2017.04.014.

[26] J. Wu, R. Petrov, S. Kölling, P. Koenraad, L. Malet, S. Godet, J. Sietsma, Micro and nanoscale characterization of complex multilayer-structured white etching layer in rails, Metals 8 (10) (2018) 749, http://dx.doi.org/10.3390/met8100749.

[27] R. Pan, Y. Chen, H. Lan, E. Shiju, R. Ren, Investigation into the microstructure evolution and damage on rail at curved tracks, Wear 504–505 (2022) http://dx.doi.org/10.1016/j.wear.2022.204420.

[28] S. Mojumder, K. Mishra, K. Singh, C. Qiu, P. Mutton, A. Singh, Effect of track curvature on the microstructure evolution and cracking in the longitudinal section of lower gauge corner flow lips formed in rails, Eng. Fail. Anal. 135 (2022) http://dx.doi.org/10.1016/j.engfailanal.2022.106117.

[29] S. Li, J. Wu, R.H. Petrov, Z. Li, R. Dollevoet, J. Sietsma, "Brown etching layer": A possible new insight into the crack initiation of rolling contact fatigue in rail steels? Eng. Fail. Anal. 66 (2016) 8–18, http://dx.doi.org/10.1016/j.engfailanal.2016.03.019.

[30] M. Messaadi, M. Steenbergen, Stratified surface layers on rails, Wear 414–415 (2018) 151–162, http://dx.doi.org/10.1016/j.wear.2018.07.019.

[31] A. Al-Juboori, H. Zhu, D. Wexler, H. Li, C. Lu, A. McCusker, J. McLeod, S. Pannila, J. Barnes, Characterisation of White Etching Layers formed on rails subjected to different traffic conditions, Wear 436–437 (2019) http://dx.doi.org/10.1016/j.wear.2019.202998.

[32] V. Mattos Ferreira, Microstructural Phenomena in Pearlitic Railway Steels (Ph.D. thesis), Delft University of Technology, 2024, http://dx.doi.org/10.4233/uuid:facb282f-74a1-446d-bbc6-5ed294602ed2.

[33] M. Steenbergen, Rolling contact fatigue in relation to rail grinding, Wear 356–357 (2016) 110–121, http://dx.doi.org/10.1016/j.wear.2016.03.015.

[34] CEN, prEN13674-1 - Railway Applications - Rail - Part 1: Vignole Railway Rails 46 kg/m and Above, European Committee for Standardization, 2023.

[35] M. Steenbergen, R. Dollevoet, On the mechanism of squat formation on train rails - Part II: Growth, Int. J. Fatigue 47 (2013) 373–381, http://dx.doi.org/10.1016/j.ijfatigue.2012.04.019.

[36] M. Steenbergen, Rolling contact fatigue: Spalling versus transverse fracture of rails, Wear 380–381 (2017) 96–105, http://dx.doi.org/10.1016/j.wear.2017.03.003.

[37] S. Wong, P. Bold, M. Brown, R. Allen, A branch criterion for shallow angled rolling contact fatigue cracks in rails, Wear 191 (1–2) (1996) 45–53, http://dx.doi.org/10.1016/0043-1648(95)06621-7.

[38] X. Deng, Z. Qian, Z. Li, R. Dollevoet, Investigation of the formation of corrugation-induced rail squats based on extensive field monitoring, Int. J. Fatigue 112 (2018) 94–105, http://dx.doi.org/10.1016/j.ijfatigue.2018.03.002.
[39] R. Masoudi Nejad, K. Farhangdoost, M. Shariati, Microstructural analysis and fatigue fracture behavior of rail steel, Mech. Adv. Mater. Struct. 27 (2) (2020) 152–164, http://dx.doi.org/10.1080/15376494.2018.1472339.
[40] R.I. Carroll, J.H. Beynon, Rolling contact fatigue of white etching layer: Part 1. Crack morphology, Wear 262 (9–10) (2007) 1253–1266, http://dx.doi.org/10.1016/j.wear.2007.01.003.
[41] J. Archard, W. Hirst, The wear of metals under unlubricated conditions, Proc. R. Soc. Lond. Ser. A. Math. Phys. Sci. 236 (1206) (1956) 397–410, http://dx.doi.org/10.1098/rspa.1956.0144.
[42] E. Wild, L. Wang, B. Hasse, T. Wroblewski, G. Goerigk, A. Pyzalla, Microstructure alterations at the surface of a heavily corrugated rail with strong ripple formation, Wear 254 (9) (2003) 876–883, http://dx.doi.org/10.1016/S0043-1648(03)00239-4.
[43] S.L. Grassie, J. Kalousek, Rail corrugation : characteristics, causes and treatments, Proc. Inst. Mech. Eng. Part F: J. Rail Rapid Transit (1993) 57–68.
[44] Z. Li, S. Li, P. Zhang, A. Núñez, R. Dollevoet, Mechanism of short pitch rail corrugation: initial excitation and frequency selection for consistent initiation and growth, Int. J. Rail Transp. (2022) http://dx.doi.org/10.1080/23248378.2022.2156402.
[45] K.H. Oostermeijer, Review on short pitch rail corrugation studies, Wear 265 (9–10) (2008) 1231–1237, http://dx.doi.org/10.1016/j.wear.2008.01.037.
[46] K.-O. Edel, Aus der Rollkontaktermüdung resultierende Lebensdauer von Eisenbahnschienen, in: Eisenbahnwesen-Seminar / Technische Universität Berlin, Institut für Land- und Seeverkehr (ILS), 12. Juni 2017, 2017, p. 37.
[47] R.I. Carroll, J.H. Beynon, Rolling contact fatigue of white etching layer. Part 2. Numerical results, Wear 262 (9–10) (2007) 1267–1273, http://dx.doi.org/10.1016/j.wear.2007.01.002.
[48] S.L. Grassie, D.I. Fletcher, E.A. Gallardo Hernandez, P. Summers, Studs: a squat-type defect in rails, Proc. Inst. Mech. Eng. Part F: J. Rail Rapid Transit 226 (3) (2011) 243–256, http://dx.doi.org/10.1177/0954409711421462.